Applied Catalysis B: Environmental 258 (2019) 117762

Contents lists available at ScienceDirect

Applied Catalysis B: Environmental

journal homepage: www.elsevier.com/locate/apcatb

Highly efficient photocatalytic hydrogen generation of g-C_3N_4-CdS sheets based on plasmon-enhanced triplet–triplet annihilation upconversion

Jiaojiao Fang[a,b,d], Yukai Chen[a,b,d], Wei Wang[b,c,d,*], Liang Fang[a,b,d], Chunhua Lu[a,b,d,*], Cheng Zhu[a,b,d], Jiahui Kou[a,b,d], Yaru Ni[a,b,d], Zhongzi Xu[a,b,d]

[a] College of Materials Science and Engineering, Nanjing Tech University, Nanjing, 210009, PR China
[b] State Key Laboratory of Materials-Orient Chemical Engineering, Nanjing Tech University, Nanjing, 210009, PR China
[c] School of Physics and Optoelectronic Engineering, Nanjing University of Information Science & Technology, Nanjing, 210044, PR China
[d] Jiangsu Collaborative Innovation Center for Advanced Inorganic Function Composites, Nanjing Tech University, Nanjing, 210009, PR China

ARTICLE INFO

Keywords:
Triplet-triplet annihilation upconversion
Au plasmon resonance
Photocatalysis
Hydrogen generation

ABSTRACT

Herein we first coupled a wide photo-response photocatalyst with plasmon-enhanced triplet – triplet annihilation upconversion (TTA-UC) nanoparticles for photocatalytic hydrogen generation. The plasmon-based enhancement of TTA-UC was achieved by introducing Au nanoparticles into the core liquid of TTA-UC nanoparticles containing platinum(II)-octaethylporphyrin and 9,10-diphenylanthracene. Au-TTA nanoparticles encapsulated by silica shells significantly increased the green-to-blue upconversion compared with TTA nanoparticles. The silica shells after further surface functionalization can conjoin with photocatalysts. To improve the stability of cadmium sulfide (CdS), graphitic carbon nitride (g-C_3N_4) was combined with CdS for g-C_3N_4-CdS heterojunctions. g-C_3N_4-CdS sheets based on Au-enhanced TTA-UC can utilize the upconverted high-energy photons and thereby realized efficient photocatalytic hydrogen production. Au-TTA nanoparticles conjoined with g-C_3N_4-CdS reached a high hydrogen production of 16.88 mmol g^{-1} under visible-light irradiation and an apparent quantum efficiency of 1.439% under green-light irradiation. The study provides a new TTA-supported upconversion-photocatalysis system enhanced by Au plasmon resonance effect for effectively hydrogen generation.

1. Introduction

As an environmentally clean energy, hydrogen has attracted significant attention in recent years. The hydrogen generation of photocatalysts through water splitting is one of the most promising methods for global energy crisis [1,2]. To develop photocatalytic hydrogen generation into practical applications, broadband absorption and good stability of photocatalysts are key issues [3,4]. High energy photons that can activate photocatalysts occupy only a small proportion of the solar energy spectrum [5–7]. Hence, regulation and enhancement of the energy of photons does play a significant role in accomplishing solar-driven photocatalysis and improving photocatalytic efficiency. In addition, it's indispensable to improve stability of photocatalysts for continuable photocatalytic hydrogen production in the practical application.

Upconversion materials can convert low energy photons to photons with high energy. They have been considered as a promising strategy to improve the utilization of solar energy [8,9]. The obtained high-energy photons from upconversion systems can sensitize UV/vis-responsive photocatalysts and effectively extend absorption spectral range of photocatalysis materials. According to the reported studies, lanthanide-doped upconversion nanoparticles have been widely applied in improving the photocatalytic degradation performance of photocatalysts [10–12], such as $NaYF_4$:Yb^{3+},Tm^{3+}/TiO_2 [13,14], g-C_3N_4-based $NaYF_4$ [15,16] and $NaYF_4$:Yb,Tm@CdS [12,17,18]. However, traditional lanthanide-doped upconversion materials show narrow absorption bands, high-power excitation threshold and low quantum efficiencies [19,20]. Surface plasmons of noble metal nanoparticles, such as Ag [21,22] and Au [7,23,24], have been integrated into upconversion materials as well for further improving the upconversion luminescence efficiency. In fact, the surface plasmon enhanced luminescence intensity of lanthanide-doped nanomaterials is still limited for promoting the photocatalytic efficiency of photocatalysts.

As a new alternative upconversion approach, triplet-triplet

* Corresponding authors at: Nanjing Tech University, Nanjing, 210009, PR China; State Key Laboratory of Materials-Orient Chemical Engineering. Nanjing University of Information Science & Technology, Nanjing, 210044, PR China.
E-mail addresses: wwang@nuist.edu.cn (W. Wang), chhlu@njtech.edu.cn (C. Lu).

https://doi.org/10.1016/j.apcatb.2019.117762
Received 4 April 2019; Received in revised form 14 May 2019; Accepted 18 May 2019
Available online 13 July 2019

annihilation upconversion (TTA-UC) has received growing attention and has been applied for organic light-emitting diodes [25–27], biological examinations [28,29] and photocatalytic fields [30–33], due to its advantages including high quantum yield, capability to upconvert low-intensity noncoherent excitation light and intense absorption coefficient [34]. TTA-UC, however, is achieved through the Dexter energy transfers between two water-insoluble organic chromophores (the sensitizer and the emitter), and the presence of oxygen can quench the upconversion fluorescence [35–37]. TTA chromophores were previously encapsulated in polymer films for isolating oxygen [38–41]. Nevertheless, TTA polymer films present low upconversion efficiency owing to the low mobility of TTA chromophores, which limits their application in photocatalytic fields. Recently, researchers mainly investigate two ways to realize the high-efficiency TTA-UC, and the photocatalytic efficiency of photocatalysts is thereby promoted. Plasmonic particles are incorporated into TTA-UC films [39,40]. Besides, chromophores are encapsulated in capsules [42,43] or silica shells [30,44] to ensure their good diffusion and deoxygenated environments. Still now, rare reports studied the plasmon-enhanced TTA nanoparticles for the stable and efficient photocatalytic hydrogen evolution [40].

In addition, the intrinsic stability of photocatalysts is important for hydrogen production performance. CdS is an attractive photocatalyst with efficient absorption of visible light due to its desired band-gap width [45]. However, the ultrafast recombination rate of photoinduced electron-hole pairs and the strong photo-corrosion still restrict the stable applications of CdS in hydrogen production [46,47]. Fabrication of heterojunctions among other photocatalysts such as CdS-TiO_2 [48], CdS-MoS_2 [49] and BiOBr-CdS [50] has been verified to effectively solve above-mentioned problems. Graphitic carbon nitride (g-C_3N_4) as a metal-free photocatalyst has gained extensive attention owing to its intrinsic photoabsorption and photoresponse [51,52]. g-C_3N_4-CdS heterojunctions can improve the chemical stability and dispersibility of CdS in g-C_3N_4 nanosheets for effective hydrogen production performance [53–55].

Herein, we developed a novel upconversion-photocatalysis system that integrated Au plasmon-enhanced TTA-UC with g-C_3N_4-CdS heterojunctions to achieve broadband spectrum-responsive and steady photocatalytic hydrogen generation. Au nanoparticles as well as TTA chromophores of platinum-octaethylporphyrin (PtOEP, the sensitizer) and 9, 10-diphenylanthracene (DPA, the emitter) were together encapsulated for the first time in a rigid silica shell. After the silica surface further functionalization, obtained g-C_3N_4-CdS heterojunctions by an in-situ precipitation reaction can attach to Au-enhanced TTA-UC nanoparticles to form upconversion-photocatalysis materials. The crystallographic phase, chemical bond environments, elemental analysis and morphology of upconversion-photocatalysis materials were studied in detail. The absorption spectra, fluorescence property, photocatalytic hydrogen production ability and photocatalytic stabilities were also investigated. The innovative design of Au-TTA-based upconversion-photocatalysis systems with broadband response and excellent stability is expected to enhance continuable photocatalytic hydrogen generation under visible light irradiation.

2. Materials and experimental

2.1. Materials

All chemicals were commercially available and used without further purification. Urea (99.7%, Xilong Chemical Reagent Co., Ltd.) was treated at 520 °C for 4 h and then was treated by thermal oxidation etching to obtain carbon nitride (C_3N_4). Cadmium acetate ($Cd(Ac)_2{\cdot}2H_2O$, 98.5%), hydrogen tetrachloroaurate (III) hydrate ($HAuCl_4{\cdot}3H_2O$, 99.9%), 9,10-diphenylanthracene (DPA, 97%, Aladdin), (3-aminopropyl)-trimethoxysilane (APTMS, 97%), oleylamine (OAm, 80–90%), oleic acid (OA, 90%, Aladdin), *tert*-butylamine-borane complex (TBAB, 95%) and tetralin (98%) were purchased from Aladdin, China. Dimethyl sulfoxide (DMSO, 99.0%, Shanghai Lingfeng Chemical Reagent CO., Ltd.) was used as the sulfur source of CdS. Tetrahydrofuran (THF, > 99%, Sinopharm Chemical Reagent Co., Ltd.), ethyl silicate (TEOS, Sinopharm Chemical Reagent Co., Ltd.), platinum (II)octaethylporphyrin (PtOEP, 95%, Frontier Scientific), chloroplatinic acid ($H_2PtCl_6{\cdot}\ 6H_2O$, Sinopharm Chemical Reagent Co., Ltd.), acetone (> 99.5%, Shanghai Lingfeng Chemical Reagent CO., Ltd.), triethanolamine (TEA, Shanghai LinFeng Chemical Reagent Co., Ltd.) and methanol (> 99.5%, WuXi City YaSheng Chemical Co., Ltd.) were used as received. Deionized (DI) water was used in all experiments.

2.2. Synthesis of silica nanoparticles composed of Au-PtOEP&DPA

Au was prepared following a typical reduction procedure as reported previously [56]. Tetralin (10 mL), OAm (10 mL), and chloroauric acid (0.1 g) were mixed and stirred for 10 min under nitrogen gas. The reducing solution of TBAB (0.5 mmol), tetralin (1 mL) and OAm (10 mL) was sonicated and injected into the aforementioned solution. The mixture was reacted at 20 °C for 1 h. After that, 60 ml acetone was added and the obtained precipitate was centrifuged at 12,000 rpm for 30 min. Subsequently, the product was washed with acetone several times and redispersed in THF.

The physical mixture of PtOEP and DPA (PtOEP&DPA) here was noted as PtDPA. Au-PtDPA-containing silica (Au-PtDPA@SiO_2) was synthesized according to a previous report method with a few modifications [44]. PtOEP (1 mmol L^{-1}) and DPA (2 mmol L^{-1}) in THF were separately prepared. OA solution with Au-PtDPA was prepared by adding PtOEP solution (2.5 mL), DPA solution (3 mL) and different volume of Au solution into 5 ml OA. The mixture was placed in an oven at 70 °C for 12 h to completely evaporate the THF. The mixture (300 μL) was mixed with 100 ml of deionized water and sonicated for emulsification. 1 mmol of APTMS was added dropwise to the emulsion. Whereafter, TEOS (1.34 mL) was injected into the mentioned solution. The final mixture was kept stirring gently at 55 °C for 48 h. After reaction, the precipitate was centrifuged and washed with deionized water. The final product was dried in a vacuum oven at 60 °C for 12 h. The samples are separately named as (0, 1%, 2%, 3%, 4%, 5% and 10%) Au-PtDPA according to the adding volume fraction of Au solution (0, 1%, 2%, 3%, 4%, 5% and 10%). The sample OA@SiO_2 was prepared by using OA solution without Au-PtDPA and other experimental procedures were the same.

2.3. Preparation of g-C_3N_4-CdS composite photocatalysts

The synthesis of g-C_3N_4-CdS followed a formerly reported method with a few modifications [57]. Urea (20 g) was put into an aluminum crucible sealed, and treated at 540 °C for 3 h to get a yellow solid. Afterwards, the solid was heated to 500 °C at a heating rate of 1 °C/min and kept at 500 °C for 2 h, following by cooling to room temperature to obtain g-C_3N_4. A varying amount of the prepared g-C_3N_4 was dispersed in 80 ml of DMSO before stirring strongly for 24 h. The obtained suspension was ultrasonicated for some time after adding 0.8 mmol of $Cd(Ac)_2{\cdot}2H_2O$. The solution was reacted at 180 °C for 12 h. After cooling to room temperature, the precipitates were collected by centrifugation, and then washed with acetone and ethanol several times. The resulting samples g-C_3N_4-CdS were dried at 60 °C for 12 h. Similarly, a series of g-C_3N_4-CdS composites with various weight ratios of g-C_3N_4 to CdS of 0%, 0.5%, 1%, 2%, 5%, 10% and 20% were prepared and are marked as CdS, NC0.5, NC1, NC2, NC5, NC10 and NC20, respectively. The pure g-C_3N_4 photocatalyst was obtained under the same conditions without adding $Cd(Ac)_2{\cdot}2H_2O$ and is named as g-C_3N_4.

2.4. Fabrication of Au-PtDPA@SiO_2/ photocatalysts hybrid samples

Au-PtDPA@SiO_2 (0.3 g) was dispersed in 90 ml of ethanol, and then 2.1 ml of APTMS was added the mentioned solution. The mixture was

kept stirring for 12 h. The obtained nanoparticles with amino groups were divided into three equal pieces and then redispersed in NC2 aqueous solution. The suspension was stirred at 60 °C for 12 h and then kept stirring under ambient temperature for 24 h. The final products with various weight ratios of NC2 to Au-PtDPA@SiO_2 of 0.1, 0.2, 0.5, 0.75 and 1 were prepared and are noted as Au-PtDPA@SiO_2@xNC2 (x = 0.1, 0.2, 0.5, 0.75 and 1). According to the same method, PtDPA@SiO_2@0.5NC2 and OA@SiO_2@0.5NC2 also were prepared for further experiment tests.

2.5. Characterization

The phase structure was measured with a SmartLab diffractometer (XRD, Rigaku, Japan), employing Cu Kα radiation (λ = 0.15406 nm) with a scanning speed of 10°/min. The absorption spectra and the diffuse reflection spectra were obtained using an UV–vis-NIR spectrophotometer (Cary 5000, Agilent Technologies, USA). The absorption spectra were converted from reflection by Kubelka-Munk method. The morphology and lattice fringes were recorded on a field emission scanning electron microscope (FESEM, SU8010, Hitachi, Japan) and transmission electron microscope (JEOL JEM-2010, Japan), respectively. FTIR spectra were conducted on a PerkinElmer model frontier spectrometer (FT-IR, Agilent Technologies, USA). The surface chemical environments were characterized by X-ray photoelectron spectroscopy (XPS, PHI-5000, Ulvac-Phi, Japan) with monochromatic Al Kα X-rays. Atomic force microscope (AFM, Dimension Icon, Bruker, USA) was used to perform the thickness and surface structure of samples. The fluorescence spectra and fluorescence lifetime spectra were acquired with a fluorescence spectrophotometer (Jobin Yvon FL3-221, HORIBA, France). Transient photocurrent responses were obtained by the electrochemical workstation (CHI660E, ChenHua, China). The hydrogen gas quantity was analyzed by the gas chromatography system (Agilent Technologies 7890B, America).

2.6. Photocatalytic performance evaluation

Photocatalysts (1 g) were separately dispersed in 100 ml deionized water containing methanol (100 μL) and H_2PtCl_6 aqueous solution (100 μL, 25 mmol L^{-1}) and then were irradiated with a 365 nm LED for 2 h to obtain co-catalyst modified photocatalysts.

The photocatalytic hydrogen evolution reaction was carried out in a quartz flash. 20 mg of co-catalyst modified photocatalysts was dispersed in 40 ml aqueous solution containing 10% TEA as sacrificial reagents. The suspension was stirred and deoxygenated by bubbling argon into the solution. Then, the system was irradiated by a xenon lamp (300 W) equipped with a UV-cut-off filter (780 nm > λ > 420 nm)/green light hand-pass optical filter.

The apparent quantum yield (AQY) was measured under the same condition. AQY was calculated as follows:

$$AQY = \frac{number\ of\ reacted\ electrons}{number\ of\ incident\ photons} \times 100\%$$
$$= \frac{number\ of\ evolved\ hydrogen\ molecules \times 2}{number\ of\ incident\ photons} \times 100\%$$

3. Results and discussion

The fabrication procedure for Au enhanced TTA-UC-photocatalysis system is illustrated in Scheme 1. The OA solution containing Au nanoparticles and chromophores was emulsified to isolate oxygen. Then TEOS hydrolysis offered a rigid silica shell to encapsulate the emulsion while keep chromophores' mobility. To achieve efficient and steady photocatalytic hydrogen generation, g-C_3N_4-CdS heterojunctions were fabricated via an in-situ hydrothermal fabrication synthetic process. The obtained ultra-thin g-C_3N_4 nanosheets by the thermal oxidation etching offered a great platform for well-dispersed CdS deposition. After the surface functionalization of silica shells, Au enhanced TTA-UC nanoparticles were attached to g-C_3N_4-CdS heterojunctions through the electrostatic interaction for the effective photocatalytic hydrogen production.

3.1. Structure and property of Au-PtDPA@SiO_2

TEM image (Fig. 1a) shows that mono-dispersed Au nanoparticles had the average diameters of 6 nm. As seen from HRTEM image (Fig. 1b), the planar spacing of nanoparticles was 0.236 nm, corresponding to the (111) planes of Au [56]. The absorption spectra of PtDPA, Au-PtDPA and Au are shown in Fig. 1c. Au had a broad MPR peak centered at 525 nm, which effectively overlapped with the characteristic absorption bands of PtOEP (centered at 500 and 535 nm) and the photoexcitation wavelength (535 nm) used in this study. In addition, the characteristic absorption cross section of PtOEP in Au-PtDPA was higher than that in PtDPA. This is because local electromagnetic fields can be generated near Au nanoparticles when Au-PtDPA is excited by light resonant with the MPR mode [39]. Furthermore, under the excitation light of 535 nm, Au-PtDPA in THF displayed the upconversion fluorescence emission of DPA centered at 425 nm and the Stokes emission of PtOEP around 643 nm, both of which are far from the plasmonic absorption of Au nanoparticles (Fig. 1d). Au nanoparticles, thus, can be considered to enhance TTA-UC by coupling the metal plasma resonance (MPR) effect to PtOEP absorption.

The average size of the obtained 3% Au-PtDPA@SiO_2 clusters by incorporating Au into chromophores was around 200 nm, as shown in Fig. 2a. Au particles with diameter of 6 nm were dispersed in the core of Au-PtDPA@SiO_2 (Fig. 2b). The interplanar distance of the lattice fringes approached 0.236 nm (the inset in Fig. 2b), which is in agreement with the analytical result from Fig. 1b. There was negligible existence of Au elements in the XPS spectrum of Au-PtDPA@SiO_2 (Fig. S1), suggesting further that Au nanoparticles were only encapsulated in the interior of Au-PtDPA@SiO_2 clusters.

As shown in Fig. 3a, the light absorption of Au-PtDPA@SiO_2 nanoparticles at the wavelength of 535 nm increased evidently in the presence of Au, due to the MPR absorption band of Au nanoparticles. Fig. 3b depicts the TTA-UC performance of Au-PtDPA@SiO_2 under the xenon lamp radiation with the light of 535 nm. The incorporation of Au into PtDPA@SiO_2 nanoparticles displayed strong blue luminescence emission at 400–450 nm (Fig. 3b). The luminescent intensity increased at first and then decreased by increasing the adulterate amount of Au (Fig. 3b), owing to the plasmonic enhanced TTA-UC at low concentrations of Au and competitive quenching of the chromophores' energy transfer by the excess Au [39]. Additionally, the upconverted emission intensity from 3% Au-PtDPA@SiO_2 reached the maximum that is 2.2-fold higher than that of TTA-UC samples without Au. Nevertheless, 3% Au-PtDPA@SiO_2 showed a weak increase in the PtOEP phosphorescence intensity (Fig. S2), verifying that the enhanced TTA-UC can be attributed mainly to the increased characteristic light absorption of PtOEP by MPR.

To further analyze the upconverted fluorescent property of samples, the log-log plots of the emission intensities versus excitation power at 425 nm are shown in Fig. 3c. The fluorescent intensities of PtDPA@SiO_2 with and without Au increased continuously by increasing excitation power. The slopes of the fitted line for PtDPA@SiO_2 and 3% Au-PtDPA@SiO_2 were 1.78 and 2.08, respectively, indicating that TTA-UC had a quadratic dependence on excitation power. The fit of 3% Au-PtDPA@SiO_2 at 425 nm produced a higher slope than that of PtDPA@SiO_2, which demonstrates that the addition of Au into PtDPA@SiO_2 increased efficient radiative transitions in the process of TTA-UC. To further probe the energy transfer process, decay lifetimes were used for uncovering the energy evolvement under excitation. As shown in Fig. 3d, the fluorescent lifetime of 3% Au-PtDPA@SiO_2 (35 μs) was slightly longer than that of PtDPA@SiO_2 (28 μs), which indicates that

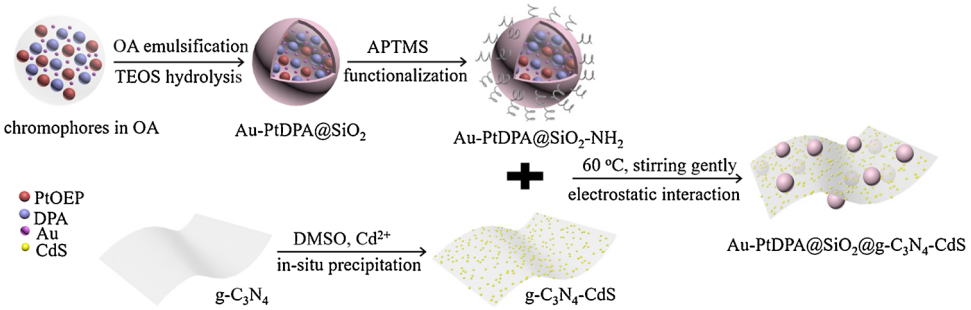

Scheme 1. Schematic illustration of the upconversion-photocatalysis system fabrication process.

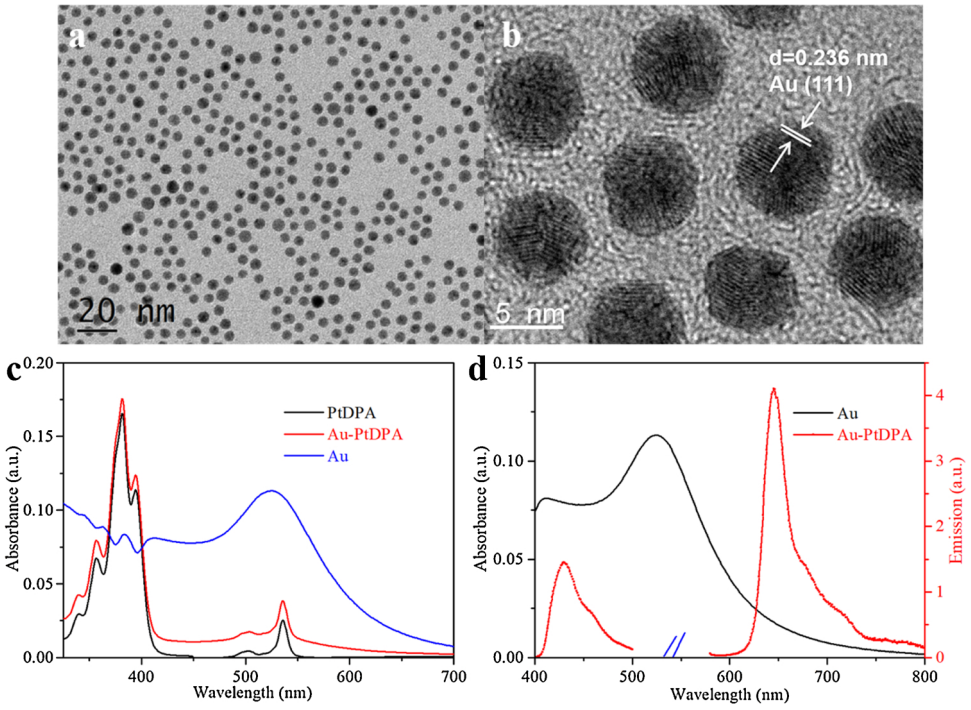

Fig. 1. (a) TEM and (b) HRTEM images of Au THF solution. (c) UV/vis absorption spectra of PtDPA, Au-PtDPA and Au dispersed separately in THF. (d) Emission spectra of Au-PtDPA in THF under xenon lamp radiation with 535 nm. The absorption spectrum of the Au in THF is shown for comparison.

the MPR of Au can improve the energy transfer efficiencies. The results of these two optic tests are complementary to the fluorescence emission spectra of composites (Fig. 3b).

3.2. Structure and property of g-C_3N_4-CdS photocatalysts

Fig. 4a shows the XRD patterns of CdS, NC2 and g-C_3N_4. Two diffraction peaks were found in g-C_3N_4, corresponding separately to the (100) and (002) planes of g-C_3N_4 [58–60]. The characteristic peaks at 26.6°, 44.1° and 52.2° are indexed to the (111), (220) and (311) planes of CdS (JCPDS 80-0019), respectively. Compared with the CdS pattern, there were negligible changes in the XRD pattern of NC2. g-C_3N_4-CdS heterojunctions did not exhibit the characteristic peaks of g-C_3N_4 (Fig. S3a), owing to the overlap of the diffraction peaks of CdS (26.6°) and g-

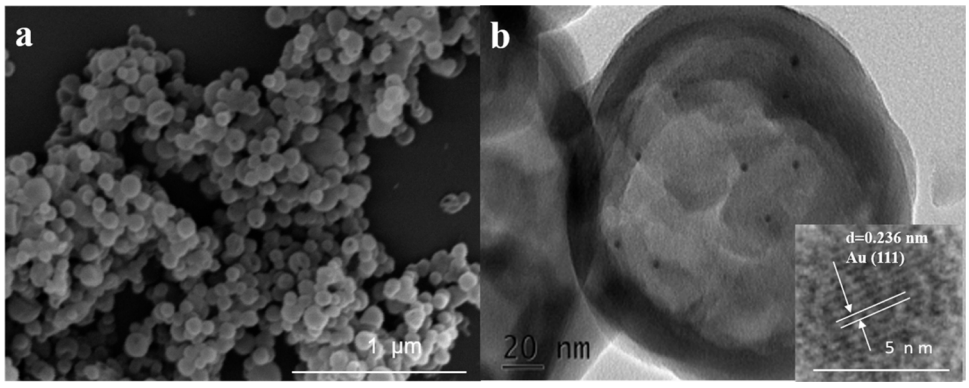

Fig. 2. (a) FESEM image and (b) TEM image of 3% Au-PtDPA@SiO_2. The inserted HRTEM image of (b) shows the detailed structure of Au in 3% Au-PtDPA@SiO_2.

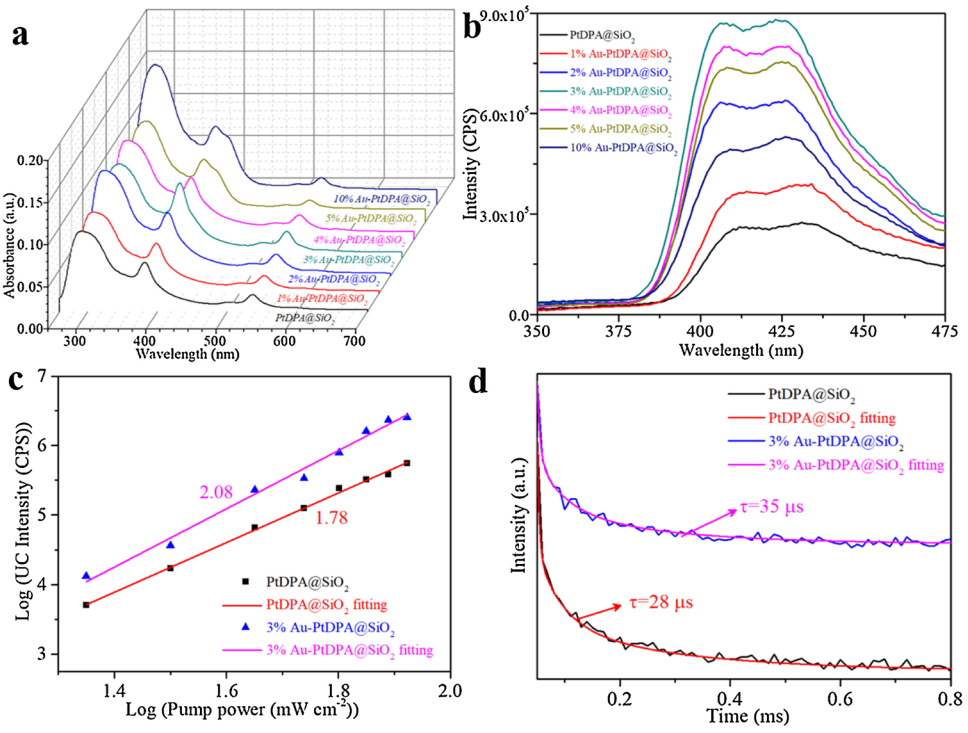

Fig. 3. (a) Absorption spectra and (b) fluorescence emission spectra of PtDPA@SiO_2 clusters with different adulterate amount of Au under the xenon lamp radiation. (Ex 535 nm). (c) Log-log plots of samples emission intensities versus excitation powers at 425 nm and (d) the UC fluorescence lifetime spectra of PtDPA@SiO_2 and 3% Au-PtDPA@SiO_2 at 425 nm.

C_3N_4 (27.4°). The characteristic bands at 1241, 1314, 1405, 1461, 1569 and 1639 cm^{-1} [61,62] correspond to the stretching vibration of C—N heterocycles in the FITR spectra of NC2 (Fig. 4b), indicating the appearance of g-C_3N_4. The similar result can also be found in the FITR spectra of heterojunctions with different weight of g-C_3N_4 (Fig. S3b). Moreover, the peaks at 2925, 1735 and 1403 cm^{-1} are separately assigned to N—H stretching vibration, C═O stretching vibrations and O—H stretching [63]. The existence of these hydrophilic groups enhanced the dispersion of g-C_3N_4-CdS in aqueous solution.

SEM and TEM images display the morphology and the structure of g-C_3N_4-CdS heterojunctions. There was a substantial aggregation of CdS nanoparticles, and the average diameter of CdS nanoparticles was about 20 nm (Fig. 5a). Fig. 5d displays g-C_3N_4 with a crumpled shape, and its thickness was approximately 2.7 nm according to AFM image (Fig. S4a). The aggregation of CdS nanoparticles reduced with the increased amount of g-C_3N_4 in heterojunctions (Fig. S5). Many decrescent CdS particles were attached uniformly on the g-C_3N_4 nanosheets as shown in the SEM and TEM images (Fig. 5b and e) and AFM image (Fig. S4b), which was caused by the interactions between CdS and g-C_3N_4. In addition, the HRTEM image (Fig. 5f) exhibits that CdS nanoparticles with the diameter of 3 nm had the lattice distances of 0.177, 0.208 and 0.337 nm. These lattices were assigned separately to the (111), (220) and (311) crystal planes of CdS, which agrees with the XRD analysis (Fig. 4a).

The optical absorption properties of samples were also determined by UV–vis absorption spectra. Fig. 6a depicts that the absorption edge of g-C_3N_4 was located at 440 nm and that CdS with the band-gap energy of 2.4 eV displayed strong and broad absorption in visible light region. Compared with g-C_3N_4, the introduction of g-C_3N_4 in CdS enhanced the visible-light absorbance of NC2. Besides, there was a slight red-shift absorption in the absorption edge of g-C_3N_4-CdS heterojunctions with different amount of g-C_3N_4 (Fig. S6). Hence, the loading of CdS on g-C_3N_4 can adjust the visible-light response of the heterojunctions to realize the efficient utilization of the solar energy.

As shown in Fig. 6b, the photoconductive properties of CdS, NC2 and g-C_3N_4 were measured by transient photocurrent responses under intermittent visible light irradiation. The photocurrent response of g-C_3N_4 reached the lowest value owing to its weak visible-light response and rapid recombination of photo-induced carriers. The addition of CdS on the 2 wt% g-C_3N_4 sheets had the highest transient photocurrent response compared with g-C_3N_4 and CdS, revealing the optimal charge separation efficiency and further promoting the photocatalytic activity.

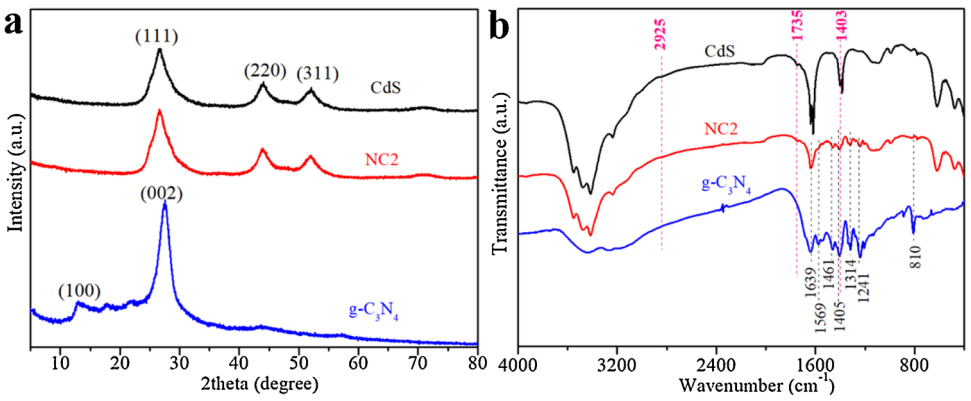

Fig. 4. (a) XRD patterns and (b) FTIR spectra of CdS, NC2 and g-C_3N_4.

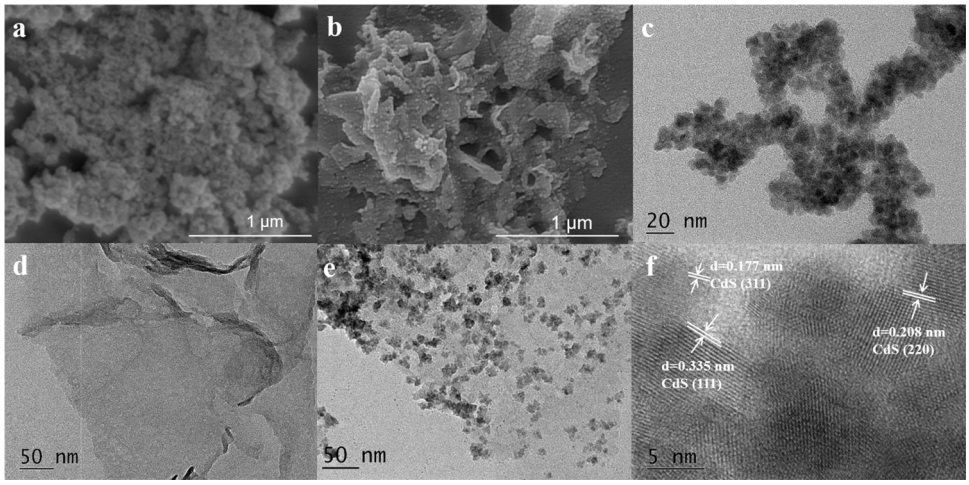

Fig. 5. FESEM images of (a) CdS and (b) NC2; TEM images of (c) CdS, (d) g-C_3N_4 and (e) NC2; (f) HRTEM image of NC2.

The hydrogen evolution of CdS coupled with different weight ratio of g-C_3N_4 was measured to investigate the photocatalytic performance. g-C_3N_4 presented only a small amount of H_2 production (0.68 mmol g^{-1} h^{-1}) as displayed in Fig. 6c. Compared with the glomerate CdS (2.37 mmol g^{-1} h^{-1}), CdS with small amount of g-C_3N_4 exhibited a relatively high H_2 production activity.

It can be attributed to that the matched bandgap position between g-C_3N_4 and CdS facilitated the valid separation of photogenerated electron-hole pairs and transfer of photogenerated electrons [53]. The heterojunction achieved the optimal hydrogen evolution rate up to 6 mmol g^{-1} h^{-1} at a loading of 2 wt% g-C_3N_4 content. Nevertheless, the photocatalytic H_2 evolution was decreased by further increasing the g-C_3N_4 content beyond 2 wt%. CdS naonoparticles were covered by the excess g-C_3N_4, leading to the less activity site exposure of CdS and weak visible-light response of composites. To evaluate the stabilities of CdS and NC2, the cycling runs for hydrogen evolution are shown in Fig. 6d. The performance of hydrogen generation for CdS fell significantly by 24.5% after five runs because of CdS photocorrosion. Compare with CdS, NC2 still possessed the excellent hydrogen producing performance of 92% after photocatalytic tests, demonstrating that the effect between CdS and g-C_3N_4 can improve the stability of heterojunctions effectively.

3.3. Structure and property of upconversion-photocatalysis hybrid samples

The crystallographic phases of upconversion-photocatalysis hybrid samples are presented in Fig. 7a. The XRD pattern of Au-PtDPA@SiO_2 displayed negligible impurity peaks except the bread-shaped peak of SiO_2, implying the low concentration of Au nanoparticles in the core of PtDPA@SiO_2. The positions of main diffraction peaks of the as-prepared upconversion-photocatalysis composites can correspond to those of NC2. Moreover, the diffraction peaks at 26.5° were broad because of their superposition with the crystalline diffraction peak of Au-PtDPA@SiO_2 (21.6°). The chemical structures of the prepared composites were analyzed by FTIR spectra (Fig. 7b). Strong Si-O peaks of Au-PtDPA@SiO_2 were detected at about 1077 cm^{-1}. The FTIR spectra of upconversion-photocatalysis composites exhibited the characteristic peaks of g-C_3N_4, CdS and Au-PtDPA@SiO_2. Compared with NC2, the bands of the hydrophilic groups (2925, 1735 and 1403 cm^{-1}) for upconversion-

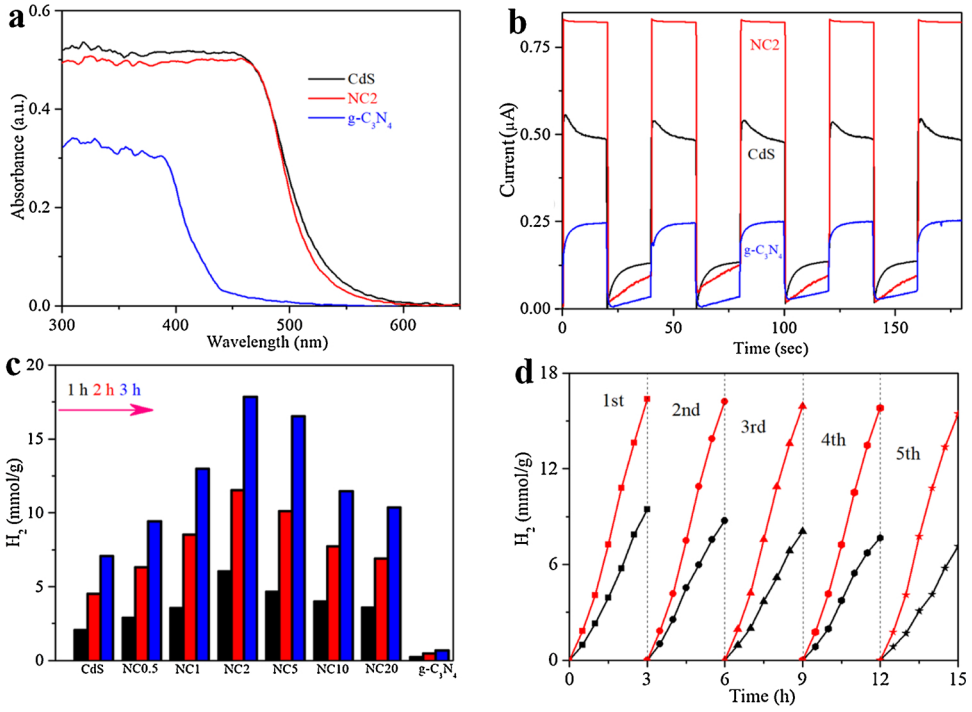

Fig. 6. (a) UV–vis absorption spectra and (b) transient photocurrent response plots of CdS, NC2 and g-C_3N_4 under visible light (λ > 420 nm). (c) The H_2 evolution rates on samples at room temperature under visible light (λ > 420 nm). (d) Cycling runs of CdS (black line) and NC2 (red line) for photocatalytic H_2 evolution (After every 3 h, the produced H_2 was evacuated.

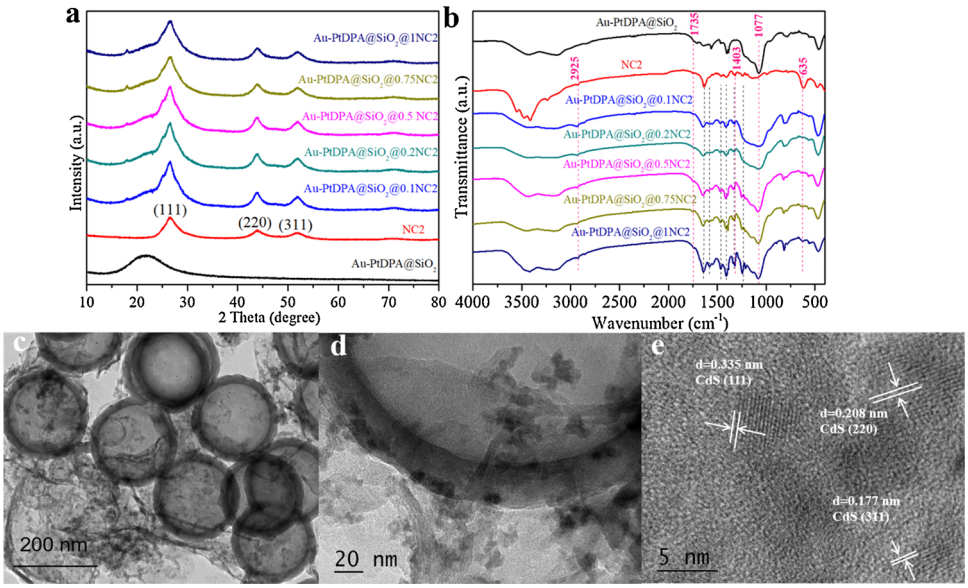

Fig. 7. (a) XRD patternsv and (b) FTIR spectra of the as-prepared composites. (c) TEM image, (d) the magnified TEM image and (e) HRTEM image of Au-PtDPA@SiO_2@0.5NC2.

photocatalysis composites presented slight red shifts, which demonstrates the presence of the interaction between Au-PtDPA@SiO_2 and NC2. In comparison with NC2, the red shifts of these bands appeared clearly in Au-PtDPA@SiO_2@0.5NC2.

The TEM images of Au-PtDPA@SiO_2@0.5NC2 are shown in Fig. 7c and d. NC2 sheets served as the support for Au-PtDPA@SiO_2, and Au-PtDPA@SiO_2@0.5NC2 stayed the intrinsic morphology of NC2 after attaching NC2 to Au-PtDPA@SiO_2 (Fig. 7e). As shown in Fig. S7, in comparison with the physical mixture of Au-PtDPA@SiO_2 and NC2 (Au-PtDPA@SiO_2/0.5NC2), the particle size of Au-PtDPA@SiO_2@0.5NC2 was increased, and there were less samples with small size, both of which indicate that Au-PtDPA@SiO_2 nanoparticles were anchored tightly on NC2. This result can also be confirmed by the AFM image (Fig. S8).

According to the UV–vis absorption spectra (Fig. 8a), Au-PtDPA@SiO_2 displayed an obvious characteristic absorption band at 535 nm before coating NC2. The absorption spectra of the composites combined with NC2 showed an enhanced absorption capacity in the visible-light region (400–450 nm), verifying that the utilization efficiency of solar light was increased. Hence, the disappearance of the characteristic absorption band (535 nm) in the composites was impacted by the absorption behavior of NC2 with the absorption band side of 522 nm. To further discuss the optical properties of the composites, the fluorescence emission spectra were characterized under the excitation light of 535 nm (Fig. 8b). Au-PtDPA@SiO_2 showed strong UC luminescence. The blue light emission at 400–450 nm was reduced greatly after combination with NC2, which should be credited to the absorption of NC2 sheets (Fig. 8a). NC2 absorbed the high-energy blue light that was generated by TTA-UC, which can be helpful to enhance visible-driven photocatalytic activity.

Photocatalytic hydrogen evolution of the composites was assessed under visible light illumination ($\lambda > 420$ nm) with TEA as the sacrificial reagent. Fig. 9a exhibits the hydrogen evolution rates of the composites. For comparison, the evolution rate of the physical mixtures of Au-PtDPA@SiO_2 and NC2 sheets with different mass percent is shown as well. Both composites and mixtures showed gradually increased hydrogen production performance by increasing the loading of NC2 sheets. The photocatalytic hydrogen production activities of Au-PtDPA@SiO_2@NC2 composites are higher than that of the corresponding physical mixtures of Au-PtDPA@SiO_2/NC2. The close contact between the photocatalysts and UC materials, thus, can highly improve the photocatalytic performance. For more clarity, the difference of hydrogen production rate between composites and mixture (ΔH_2) is shown in Fig. 9b. The amount of NC2 might be too low to fully couple with UC clusters, and then the high-energy photons from Au-PtDPA@SiO_2 might not be absorbed completely and used by photocatalysts for hydrogen production. Therefore, ΔH_2 was improved mildly to 0.65 mmol g^{-1} h^{-1} when the content of NC2 was 20%, and the optimal photocatalytic activity was achieved at 50% NC2 sheets (ΔH_2 reached a maximum of 2.76 mmol g^{-1} h^{-1}). The excess introduction of NC2

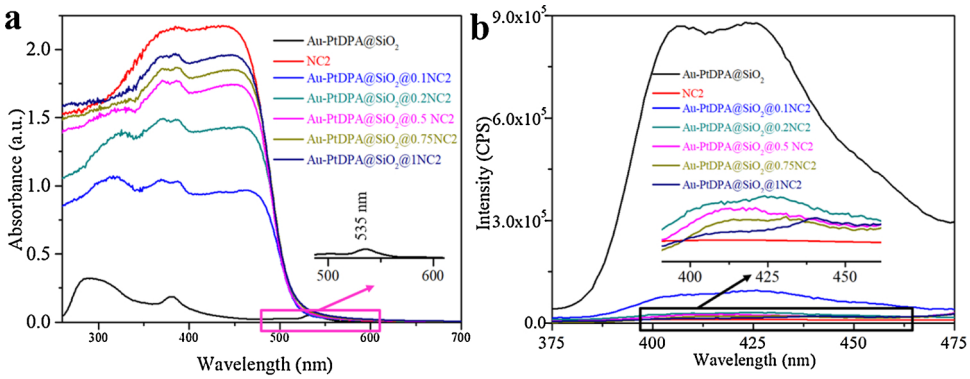

Fig. 8. (a) UV–vis absorption spectra and (b) the fluorescence emission spectra (Ex 535 nm) of composites.

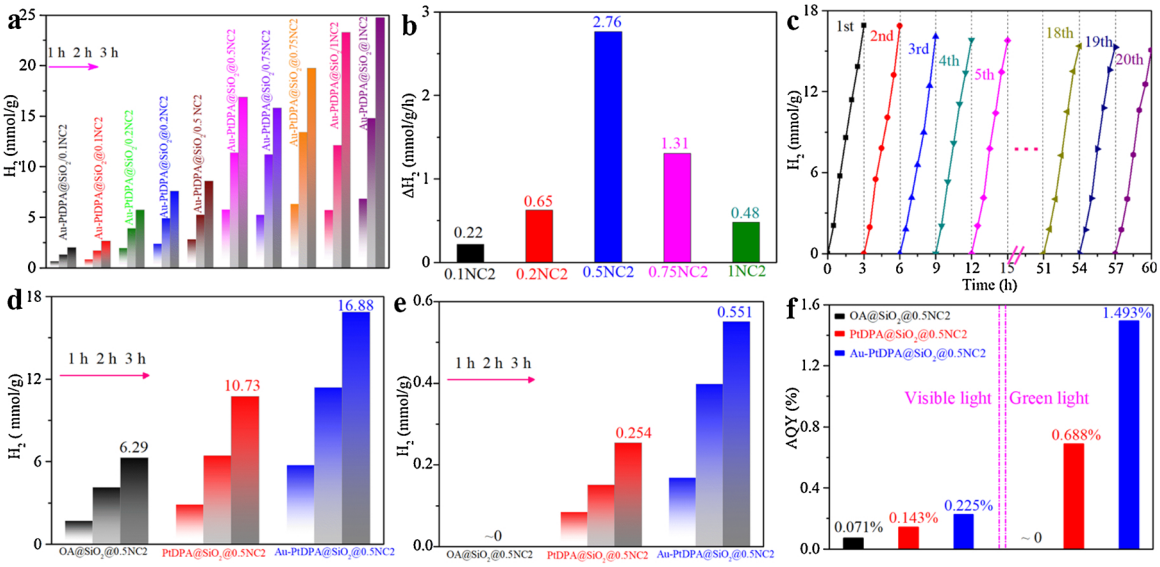

Fig. 9. (a) The hydrogen evolution amount on the composite and mixtures at room temperature under visible light; (b) The differences of the hydrogen evolution rate between the composite and mixtures, calculated from Fig. 9a; (c) Cycling runs of Au-PtDPA@SiO_2@0.5NC2 for photocatalytic hydrogen evolution under visible light irradiation. The hydrogen evolution amount on composites at room temperature (d) under visible light and (e) under green light; (f) The apparent quantum efficiency of hydrogen evolution of composites.

limited the absorption of excitation light of UC materials and accordingly reduced the upconversion intensity (Fig. 8b). The photocatalytic activity, thus, was deteriorated. The durability test of hydrogen production was performed on Au-PtDPA@SiO_2@0.5NC2 to evaluate its stability of photocatalytic activities. As shown in Fig. 9c, the hydrogen production performance of Au-PtDPA@SiO_2@0.5NC2 still stayed more than 90% after 20 runs. Moreover, its crystalline phase after the cycling runs changed negligibly as shown in Fig. S9, indicating its structural stability.

To confirm TTA-upconversion enhanced photocatalysis, we investigated the photocatalytic activities of OA@SiO_2@0.5NC2, PtDPA@SiO_2@0.5NC2 and Au-PtDPA@SiO_2@0.5NC2. Due to the absence of light conversion performance, OA@SiO_2@0.5NC2 exhibited an inferior photocatalytic hydrogen rate that is equivalent to the H_2 production rate of pure NC2 sheets under visible light irradiation. The photocatalytic hydrogen production was increased by 70.6% from 6.29 to 10.73 mmol g^{-1} after the replacement of OA@SiO_2 by PtDPA@SiO_2 (Fig. 9d), implying that the obtained high energy photons through TTA-UCL process can effectively enhance the photocatalytic activity. The incorporation of Au nanoparticles into the TTA-UC materials enhanced notably the hydrogen production performance of the photocatalytic composite. Compared with OA@SiO_2@0.5NC2 and PtDPA@SiO_2@0.5NC2, Au-enhanced TTA-UC improved the hydrogen production efficiency of Au-PtDPA@SiO_2@0.5NC2 (16.88 mmol g^{-1}) by about 168% and 57%, respectively. Moreover, the AQY of hydrogen evolution over Au-PtDPA@SiO_2@0.5NC2 is 3.17 folds as high as that of OA@SiO_2@0.5NC2 (Fig. 9f).

The hydrogen evolution amount on the composite were also studied under green light irradiation (Fig. 9e). Compared with OA@SiO_2@0.5NC2 that had no hydrogen production, the AQY of PtDPA@SiO_2@0.5NC2 attaches to 0.688% (Fig. 9f), which can be attribute to the effective sensitization of NC2 from obtained higher energy photons based on TTA-UCL process. In the presence of Au, the hydrogen production reached the highest value of 0.551 mmol g^{-1} with the AQY of 1.493%. The hydrogen evolution amount of Au-PtDPA@SiO_2@0.5NC2 exceeds that of PtDPA@SiO_2@0.5NC2 by a factor of 1.17, confirming further that the enhanced blue emissions from Au-enhanced TTA-UCL can improve effectively further the photocatalytic activity of NC2.

The enhanced photocatalysis process by coupling g-C_3N_4@CdS with Au-enhanced TTA-UC nanoparticles is illustrated in Scheme 2. The low-energy green light from solar spectrum can excite the TTA-UC materials, and the addition of Au nanoparticles can further improve the UC efficiency owing to the MPR enhanced absorption of the excitation light. In addition, g-C_3N_4 was chosen to load with CdS to solve the aggregation and photocorrosion of CdS nanoparticles. Under irradiation, both of CdS and g-C_3N_4 can produce photogenerated electrons and holes. Because the band structures between CdS and g-C_3N_4 are well-matched and overlapped (Fig. S10), the photogenerated holes of CdS can be captured by g-C_3N_4. The holes in the valence band of g-C_3N_4 can oxidize further the sacrificial agent TEA. The photo-induced electrons of g-C_3N_4 can be transferred effectively to CdS, and the electrons in the valence band of CdS are transfer to the noble metal Pt for proton reduction to hydrogen. More importantly, owing to the bandgap and structure of the heterojunctions g-C_3N_4@CdS, the increased high-energy photons from Au-enhanced TTA-UC can sensitize effectively g-C_3N_4@CdS. Under the excitation of Au-enhanced TTA-UC emissions, the activated g-C_3N_4@CdS can improve separations of electron-hole pairs and thereby enhance significantly hydrogen producing performance.

4. Conclusions

In summary, this study presented the high energetic photons-driven photocatalysis by the enhanced TTA-UCL process. Incorporating PtOEP &DPA chromophores and 3% Au nanoparticles into silica shells had a 2.2-fold enhancement in the upconversion intensity of green to blue emission compared with the structure without Au, owing to an increase in the excitation-light absorption of 535 nm by the plasma resonance effect of Au. The encapsulated core-shell structure for Au-TTA nanoparticles provided vast sites to couple with stable and broad-band responsive photocatalysts (g-C_3N_4@CdS sheets) by surface functionalization. Because of high energetic photons-driven photocatalysis by TTA-UCL process, the hydrogen production ability of Au-PtDPA@SiO_2@0.5NC2 had a 1.68-fold enhancement than that of OA@SiO_2@0.5NC2 under visible light irradiation. After 20 runs, the hydrogen generation performance of Au-PtDPA@SiO_2@0.5NC2 still stayed more than 90%. Under green light irradiation, the hydrogen production of Au-PtDPA@SiO_2@0.5NC2 increased by 1.17 folds compared with PtDPA@SiO_2@0.5NC2, which can be attributed to Au-plasma enhanced emission of high-energy photons during the TTA-UCL process.

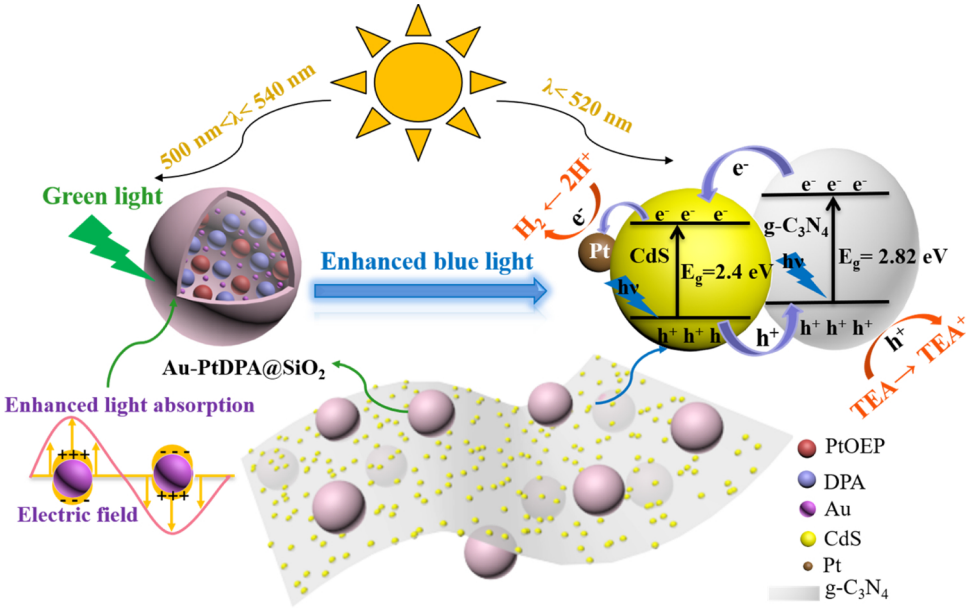

Scheme 2. Illustrative representation of the photocatalysis mechanism of g-C_3N_4@CdS based on the Au-enhanced TTA-UCL process.

Moreover, the introduction of Au in PtDPA@SiO_2@0.5NC2 resulted in an optimal AQY of 1.439%. This work offers a distinctive strategy to fabricate the plasmon-enhanced upconversion-photocatalysis system for stable and efficient water splitting to produce hydrogen.

Declarations of interest

None.

Acknowledgements

This work was supported by the National Natural Science Foundation of China (No.51502143), Natural Science Foundation of Jiangsu Province (No.BK20150919), Key University Science Research Project of Jiangsu Province (No.15KJB430022), and the Startup Foundation for Introducing Talent of NUIST (2014r037), General Project of Youth Science Foundation of Jiangsu Province China (SBK2015043512), Natural Science Foundation of Jiangsu Province (No. BK20141459), Project on the Integration of Industry, Education and Research of Jiangsu Province (No. BY2015005-16, BK20150919), Qing Lan Project, Six Talent Peaks Project in Jiangsu Province (No. XCL-029), Postgraduate Research & Practice Innovation Program of Jiangsu Province (No. KYCX17 0990) and the Project Funded by the Priority Academic Program Development of the Jiangsu Higher Education Institutions (PAPD).

Appendix A. Supplementary data

Supplementary material related to this article can be found, in the online version, at doi:https://doi.org/10.1016/j.apcatb.2019.117762.

References

[1] W. Liu, L. Cao, W.R. Cheng, Y.J. Cao, X.K. Liu, W. Zhang, X.L. Mou, L. Jin, X.S. Zheng, W. Che, Q.H. Liu, T. Yao, S.Q. Wei, Angew. Chem. Int. Ed. 129 (2017) 9440–9445.
[2] Y.X. Liu, G.F. Zhao, D.S. Wang, Y.D. Li, Natl. Sci. Rew. 2 (2015) 150–166.
[3] Y.X. Liu, G.F. Zhao, P.Y. Yu, S.S. Mao, Science. 331 (2011) 746–749.
[4] J. Liu, Y. Liu, Y.Z. Han, X. Zhang, Y. Lifshitz, S.T. Lee, J. Zhong, Z.H. Kang, Science. 347 (2015) 970–974.
[5] Y.N. Tang, W.H. Di, X.S. Zhai, R.Y. Yang, W.P. Qin, ACS Catal. 3 (2013) 405–412.
[6] Z.B. Wu, X.Z. Yuan, G.M. Zeng, L.B. Jiang, H. Zhong, Y.C. Xie, H. Wang, X.H. Chen, H. Wang, Appl. Catal. B: Environ. 225 (2018) 8–21.
[7] D.D. Li, S.H. Yu, H.L. Jiang, Adv. Mater. 30 (2018) 1707377.
[8] F. Wang, X.G. Liu, Chem. Soc. Rev. 38 (2009) 976–989.
[9] X.D. Wang, R.R. Valiev, T.Y. Ohulchanskyy, H. Ågren, C.H. Yang, G.Y. Chen, Chem. Soc. Rev. 46 (2017) 4150–4167.
[10] W. Wang, W.J. Huang, Y.R. Ni, C.H. Lu, Z.Z. Xu, ACS Appl. Mater. Inter. 6 (2014) 340–348.
[11] Q.Z. Zhang, J.J. Deng, Z.H. Xu, M. Chaker, D.L. Ma, ACS Catal. 7 (2017) 6225–6234.
[12] M.J. Tou, Y.Y. Mei, S. Bai, Z.G. Luo, Y. Zhang, Z.Q. Li, Nanoscale. 8 (2016) 553–562.
[13] Y.D. Yang, P.W. Zhou, W. Xu, S. Xu, Y.D. Jiang, X. Chen, H.W. Song, J. Mater. Chem. C 4 (2016) 659–662.
[14] Z.L. Qiu, J. Shu, D.P. Tang, Anal. Chem. 90 (2018) 1021–1028.
[15] M.Z. Huang, B.L. Yuan, L.Y. Dai, M.L. Fu, J Colloid Inter. Sci. 460 (2015) 264–272.
[16] E.J. Cheng, S.Q. Zhou, M.H. Li, Z.Q. Li, Appl. Surf. Sci. 410 (2017) 383–392.
[17] C.H. Li, F. Wang, J. Zhu, J.C. Yu, Appl. Catal. B: Environ. 100 (2010) 433–439.
[18] X.Y. Guo, W.H. Di, C.F. Chen, C.X. Liu, X. Wang, W.P. Qin, Dalton Trans. 43 (2014) 1048–1054.
[19] T.F. Schulzea, T.W. Schmidt, Energy Environ. Sci. 8 (2015) 103–125.
[20] S. Wu, H.J. Butt, Adv. Mater. 28 (2016) 1208–1226.
[21] W. Xu, H.W. Song, X. Chen, H.Y. Wang, S.B. Cui, D.L. Zhou, P.W. Zhou, S. Xu, Chem. Commun. 51 (2015) 1502–1505.
[22] D.G. Yin, X.Z. Cao, L. Zhang, J.X. Tang, W.F. Huang, Y.L. Han, M.H. Wu, Dalton Trans. 44 (2015) 11147–11154.
[23] H.Y. Xing, W.B. Bu, S.J. Zhang, X.P. Zheng, M. Li, F. Chen, Q.J. He, L.P. Zhou, W.J. Peng, Y.Q. Hua, J.L. Shi, Biomaterials. 33 (2012) 1079–1089.
[24] D.M. Wu, A. García-Etxarri, A. Salleo, J.A. Dionne, J. Phys. Chem. Lett. 5 (2014) 4020–4031.
[25] H. Fukagawa, T. Shimizu, N. Ohbe, S. Tokito, K. Tokumaru, H. Fujikake, Org. Electron. 13 (2012) 1197–1203.
[26] D.Y. Kondakov, Phil. Trans. R. Soc. A 373 (2015) 1–16.
[27] D. Di, L. Yang, J.M. Richter, L. Meraldi, R.M. Altamimi, A.Y. Alyamani, D. Credgington, K.P. Musselman, J.L. MacManus-Driscoll, R.H. Friend, Adv. Mater. 29 (2017) 1605987.
[28] B. Tian, Q.H. Wang, Q.Q. Su, W. Feng, F.Y. Li, Biomaterials. 112 (2017) 10–19.
[29] L. Huang, Y. Zhao, H. Zhang, K. Huang, J.Y. Yang, G. Han, Angew. Chem. Int. Ed. 56 (2017) 14400–14404.
[30] J.J. Fang, W. Wang, C. Zhu, L. Fang, J.Y. Jin, Y.R. Ni, C.H. Lu, Z.Z. Xu, Appl. Catal. B: Environ. 217 (2017) 100–107.
[31] A. Monguzzi, A. Oertel, D. Braga, A. Riedinger, D.K. Kim, P.N. Knüsel, A. Bianchi, M. Mauri, R. Simonutti, D.J. Norris, F. Meinardi, ACS ACS Appl. Mater. Inter. 9 (2017) 40180–40186.
[32] S. Chandrasekaran, Y.T. Ngo, L. Sui, E.J. Kim, D.K. Dang, J.S. Chung, S.H. Hur, Dalton Trans. 46 (2017) 13912–13919.
[33] O.S. Kwon, J. Kim, J.K. Cho, J. Kim, ACS Appl. Mater. Inter. 7 (2015) 318–325.
[34] V. Gray, K. Moth-Poulsen, B. Albinsson, M. Abrahamsson, Coord. Chem. Rev. 362 (2018) 54–71.
[35] J.Z. Zhao, W.H. Wu, J.F. Sun, S. Guo, Chem. Soc. Rev. 42 (2013) 5323–5351.
[36] P.L. Dos Santos, M.K. Etherington, A.P. Monkman, J. Mater. Chem. C 6 (2018) 4842–4853.
[37] L. Latterini, G. Massaro, M. Penconi, P.L. Gentili, C. Roscini, F. Ortica, Dalton Trans. 47 (2018) 8557–8565.
[38] Z. Jiang, M. Xu, F.Y. Li, Y.L. Yu, J. Am. Chem. Soc. 135 (2013) 16446–16453.
[39] K. Poorkazem, A.V. Hesketh, T.L. Kelly, J. Phys. Chem. C 118 (2014) 6398–6404.

[40] H. Kim, S. Weon, H. Kang, A.L. Hagstrom, O.S. Kwon, Y. Lee, W. Choi, J. Kim, Environ. Sci. Technol. 50 (2016) 11184–11192.
[41] J. Kim, F. Deng, F.N. Castellano, J. Kim, Chem. Mater. 24 (2012) 2250–2252.
[42] K. Katta, D. Busko, Y. Avlasevich, R. Muñoz-Espí, S. Baluschev, K. Landfester, Macromol. Rapid Commun. 36 (2015) 1084–1088.
[43] J. Kim, J. Kim, ACS Photonics 2 (2015) 633–638.
[44] O.S. Kwon, J. Kim, J.K. Cho, J. Kim, ACS Appl. Mater. Interfaces 7 (2014) 318–325.
[45] Y. Hu, X.H. Gao, L. Yu, Y.R. Wang, J.Q. Ning, S.J. Xu, X.W. Lou, Angew. Chem. Int. Ed. 52 (2013) 5636–5639.
[46] N.Z. Bao, L.M. Shen, T. Takata, K. Domen, Chem. Mater. 20 (2008) 110–117.
[47] L. Zhang, X.L. Fu, S.G. Meng, X.L. Jiang, J.H. Wang, S.F. Chen, J. Mater. Chem. A 3 (2015) 23732–23742.
[48] K. Zhao, Z.M. Wu, R. Tang, Y.D. Jiang, Y.X. Lu, Res. Chem. Intermed. 41 (2015) 4405–4411.
[49] S. Ma, J. Xie, J.Q. Wen, K.L. He, X. Li, W. Liu, X.C. Zhang, Appl. Surf. Sci. 391 (2017) 580–591.
[50] Y.X. Guo, H.W. Huang, Y. He, N. Tian, T.R. Zhang, P.K. Chu, Q. An, Y.H. Zhang, Nanoscale 7 (2015) 11702–11711.
[51] X.C. Wang, K. Maeda, A. Thomas, K. Takanabe, G. Xin, J.M. Carlsson, K. Domen, M. Antonietti, Nat. Mater. 8 (2008) 76–80.
[52] S.C. Yan, Z.S. Li, Z.G. Zou, Langmuir 25 (2009) 10397–10401.
[53] J. Fu, B.B. Chang, Y.L. Tian, F.N. Xi, X.P. Dong, J. Mater. Chem. A 1 (2013) 3083–3090.
[54] H.G. Yu, F.Y. Chen, F. Chen, X.F. Wang, Appl. Surf. Sci. 358 (2015) 385–392.
[55] R.Y. Zhang, K. Huang, H.H. Wei, D. Wang, G. Ou, N. Hussain, Z.Y. Huang, C. Zhang, H. Wu, Dalton Trans. 47 (2018) 1417–1421.
[56] S. Peng, Y. Lee, C. Wang, H.F. Yin, S. Dai, S.H. Sun, Nano Res. 1 (2008) 229–234.
[57] S.W. Cao, Y.P. Yuan, J. Fang, M.M. Shahjamali, F.Y.C. Boey, J. Barber, S.C. Joachim Loo, C. Xue, Int. J. Hydrogen Energ. 38 (2013) 1258–1266.
[58] D.Q. Gao, Q. Xu, J. Zhang, Z.L. Yang, M.S. Si, Z.J. Yan, D.S. Xue, Nanoscale. 6 (2014) 2577–2581.
[59] Y.P. Yuan, W.T. Xu, L.S. Yin, S.W. Cao, Y.S. Liao, Y.Q. Tng, C. Xue, Int. J Hydrogen Energ. 38 (2013) 13159–13163.
[60] J.L. Yuan, Y.H. Tang, X.Y. Yi, C.B. Liu, C. Li, Y.X. Zeng, S.L. Luo, Appl. Catal. B: Environ. 251 (2019) 206–212.
[61] S.B. Yang, Y.J. Gong, J.S. Zhang, L. Zhan, L.L. Ma, Z.Y. Fang, R. Vajtai, X.C. Wang, P.M. Ajayan, Adv. Mater. 25 (2013) 2452–2456.
[62] J.L. Yuan, X. Liu, Y.H. Tang, X.Y. Yi, L.L. Wang, S.Q. Zhang, T. Cai, Y.T. Liu, S.L. Luo, Y. Pei, C.B. Liu, Appl. Catal. B: Environ. 237 (2018) 24–31.
[63] L. Liu, P.R. Hu, W.Q. Cui, X.G. Li, Z.S. Zhang, Int. J. Hydrogen Energ. 42 (2017) 17435–17445.

Update

Applied Catalysis B: Environmental

Volume 271, Issue , 15 August 2020, Page

DOI: https://doi.org/10.1016/j.apcatb.2019.118155

Applied Catalysis B: Environmental 271 (2020) 118155

Contents lists available at ScienceDirect

Applied Catalysis B: Environmental

journal homepage: www.elsevier.com/locate/apcatb

Corrigendum to "Highly Efficient Photocatalytic Hydrogen Generation of g-C_3N_4-CdS Sheets Based on Plasmon-Enhanced Triplet–Triplet Annihilation Upconversion" [Applied Catalysis B: Environmental 258 (2019) /117762]

Jiaojiao Fang[a,b,d], Yukai Chen[a,b,d], Wei Wang[b,c,d,*], Liang Fang[a,b,d], Chunhua Lu[a,b,d,*], Cheng Zhu[a,b,d], Jiahui Kou[a,b,d], Yaru Ni[a,b,d], Zhongzi Xu[a,b,d]

[a] College of Materials Science and Engineering, Nanjing Tech University, Nanjing, 210009, PR China
[b] State Key Laboratory of Materials-Orient Chemical Engineering, Nanjing Tech University, Nanjing, 210009, PR China
[c] School of Physics and Optoelectronic Engineering, Nanjing University of Information Science & Technology, Nanjing, 210044, PR China
[d] Jiangsu Collaborative Innovation Center for Advanced Inorganic Function Composites, Nanjing Tech University, Nanjing, 210009, PR China

The authors regret "There is a corrigendum about Fig. 6s in the Supporting Information".

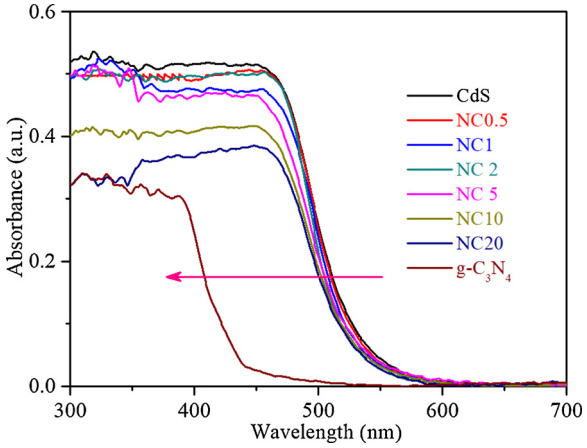

The authors would like to apologise for any inconvenience caused.

DOI of original article: https://doi.org/10.1016/j.apcatb.2019.117762
* Corresponding authors at: Nanjing Tech University, Nanjing, 210009, PR China.
E-mail addresses: wwang@nuist.edu.cn (W. Wang), chhlu@njtech.edu.cn (C. Lu).

https://doi.org/10.1016/j.apcatb.2019.118155

Available online 27 February 2020